catalysts

MDPI

Article

Synthesis of Bimetallic Pd/Pt Truncated Nanocubes and Their Catalytic Performance in Selective Hydrogenation of Acetophenone

Jingjing Bai, Xinkai Yang, Jianyu Chen, Bin Yue, Xueying Chen * and Heyong He

Department of Chemistry and Shanghai Key Laboratory of Molecular Catalysis and Innovative Materials, Fudan University, Shanghai 200438, China; 23210220001@m.fudan.edu.cn (J.B.); 21210220052@m.fudan.edu.cn (X.Y.); 22110220007@m.fudan.edu.cn (J.C.); yuebin@fudan.edu.cn (B.Y.); heyonghe@fudan.edu.cn (H.H.)

* Correspondence: xueyingchen@fudan.edu.cn; Tel.: +86-21-31242978

Abstract: A series of bimetallic Pd/Pt truncated nanocube catalysts with similar morphologies and particle sizes but different platinum contents were successfully synthesized using a colloidal method without using any capping agents. Their hydrogenation properties were systematically studied and compared with their monometallic Pd or Pt nanocrystal counterparts. The results of EDX-mapping and line scanning show that platinum was relatively uniformly distributed on the surface of the Pd/Pt bimetallic nanocrystals and was not selectively deposited at the corners of the nanocrystals. The results of the selective hydrogenation of acetophenone demonstrate that the hydrogenation rate and the carbonyl selectivity of bimetallic Pd/Pt truncated nanocube catalysts are generally much higher than those of their monometallic Pd or Pt nanocrystal counterparts. It was found that the electronic interaction between palladium and platinum in the bimetallic Pd/Pt truncated nanocube catalysts and the corresponding hydrogenation activity in the selective hydrogenation of acetophenone are closely related to the molar ratio between platinum and palladium and the thickness of the platinum layer in the bimetallic Pd/Pt truncated nanocube catalyst. With an increase in the Pt/Pd molar ratio in the bimetallic Pd/Pt truncated nanocube catalysts, the activity and carbonyl selectivity in the acetophenone hydrogenation reaction increase first, reach a maximum when the molar ratio of Pt/Pd is 0.02 and the theoretical thickness of Pt is 1.3 atomic layers, and then decrease with a further increase in the Pt/Pd ratio. The hydrogenation rate of acetophenone on the $Pd/Pt_{0.02}$ catalyst reaches 1.07×10^3 mmol·h^{-1}·$g_{cat.}{}^{-1}$, which is 79 and 75 times larger than that of the monometallic Pd and Pt nanocrystal catalysts, respectively. The maximum yield of the target product 1-phenylethanol on the $Pd/Pt_{0.02}$ truncated nanocube catalyst reaches 97.2%, which is 6.6% and 16.7% higher than that of the monometallic Pd and Pt nanocrystal catalysts, respectively.

Keywords: Pd/Pt; bimetallic nanocrystals; shape control; selective hydrogenation; acetophenone

check for updates

Citation: Bai, J.; Yang, X.; Chen, J.; Yue, B.; Chen, X.; He, H. Synthesis of Bimetallic Pd/Pt Truncated Nanocubes and Their Catalytic Performance in Selective Hydrogenation of Acetophenone. *Catalysts* **2024**, *14*, 900. https://doi.org/10.3390/catal14120900

Academic Editor: Dinesh Kumar

Received: 9 November 2024
Revised: 3 December 2024
Accepted: 4 December 2024
Published: 8 December 2024

Copyright: © 2024 by the authors. Licensee MDPI, Basel, Switzerland. This article is an open access article distributed under the terms and conditions of the Creative Commons Attribution (CC BY) license (https://creativecommons.org/licenses/by/4.0/).

1. Introduction

Bimetallic nanocrystal catalysts are a new type of catalytic materials, whose catalytic activity, selectivity, and stability are improved compared with those of their corresponding one-component metal catalysts due to the synergy and ligand effects of the two metals [1–7]. For example, in electrocatalytic reactions, bimetallic catalysts can take advantage of the stress caused by lattice mismatches between the two metals and the ligand effect to adjust the d-band center of the catalyst to increase the activity of the catalyst [6,8,9]. Metal palladium and metal platinum have important applications in both heterogeneous catalysis and electrocatalytic reactions under mild conditions [10–12]. Both metals have a face-centered cubic stacked metal structure (fcc), and their unit cell parameters differ by only 0.77%. Therefore, Pd and Pt have strong mutual coupling, which can improve the performance of

catalysts [13,14]. It has been reported that in Pd/Pt bimetallic nanocrystal catalysts, Pt usually only needs a few atomic layers of thickness to maximize catalytic activity [15–17]. The reported Pd/Pt bimetallic nanocrystals exhibit diverse morphologies, various Pd/Pt molar ratios, and significant differences in catalytic performance [18–21]. Chen and co-workers synthesized Pd-Pt octapods, tesseracts, and nanoframes; studied their electrocatalytic activities in the oxygen reduction reaction; and found that Pd-Pt tesseracts exhibited the highest level of mass activity [18]. Wang and co-workers synthesized Pd@Pt octahedra, rhombic dodecahedra, and nanocubes by means of a seed-mediated method and applied them in the electrocatalytic oxidation reaction of d-glucose [19]. For transient catalysis, the current density and sensitivity to d-glucose are in the following order: Pd@Pt octahedra > nanocube > rhombic dodecahedra [19]. Zhang and co-workers prepared Pd-Pt concave polyhedra by controlling the molar ratio of Pd and Pt precursors and found that Pd_{93}-Pt_7 exhibited the best electrocatalytic activity in methanol electro-oxidation [20].

Although Pd/Pt bimetallic nanocrystal catalysts have been systematically studied and widely used in the field of electrocatalysis, they have been reported on relatively rarely in the field of heterogeneous catalysis. Zhang and co-workers reported on kinetically stabilized small Pd@Pt core–shell nanoparticles, which exhibited enhanced catalytic performance in the hydrogenation of p-chloronitrobenzene [15]. Li and co-workers prepared Pt/Pd nanoparticles stabilized with octa(diacetic aminophenyl)silsesquioxanes (OAAPS), which exhibited a much higher level of activity than their monometallic counterparts in the hydrogenation of benzaldehyde to benzyl alcohol under mild conditions [22]. Cui and co-workers synthesized Pd-Pt bimetallic nanocatalysts loaded onto SiO_2 using a co-impregnation method, which exhibited an excellent hydrogenation degree and selectivity for C=C bonds [23].

The selective hydrogenation of acetophenone is an important reaction in industry since it is atom-economic, and the aimed-for product 1-phenylethanol is widely used in pharmaceutics and fragrance [24–31]. In our previous work, we successfully synthesized three types of surface-clean palladium nanocrystal catalysts enclosed by different crystal facets using a colloidal method without any capping agents and studied the correlation between different Pd facets and the selective hydrogenation performance of acetophenone [31]. However, the activity of the synthesized palladium nanocrystal catalyst and the selectivity for 1-phenylethanol still need to be further improved. Therefore, in order to solve the above problems, in the present work, we tentatively synthesized a series of bimetallic Pd/Pt truncated nanocube catalysts with different Pd/Pt ratios by a colloidal method in the absence of capping agents, hoping to improve catalytic performance in the selective hydrogenation of acetophenone by the introduction of Pt content. The effect of platinum content in bimetallic Pd/Pt truncated nanocube catalysts on catalytic activity and carbonyl selectivity in the selective hydrogenation of acetophenone was systematically studied.

2. Results and Discussion

2.1. Characterization of Monometallic Pd or Bimetallic Pd/Pt Truncated Nanocube Catalysts with Different Platinum Contents

Transmission electron microscopic (TEM), field-emission scanning electron microscopic (FESEM), selected-area electron diffraction (SAED), and high-resolution TEM (HRTEM) images of the monometallic Pd truncated nanocube catalyst (denoted as $Pd_{trunc\text{-}cube}$) are shown in Figure 1. The statistical results of the particle size distribution shown in the inset in Figure 1a indicate that the average particle size of the palladium truncated nanocube is ~51 nm. From the FESEM image (Figure 1b), it can be clearly observed that the palladium truncated nanocube exposes three different crystal facets, which can be regarded as a cube with eight vertices and twelve edges truncated. The typical SAED pattern of the Pd truncated nanocube oriented along the [100] direction (Figure 1c) shows square diffraction spots, corresponding to the {200} reflections of fcc Pd with d-spacings of 0.20 nm. All the projection angles between adjacent facets measured in the truncated nanocube lying flat on the TEM copper grid are ~135°, as shown in the inset in Figure 1c. This indicates that

the main facets exposed in the truncated nanocube are {100} and {110} facets, which is further verified by the corresponding HRTEM image with clearly observed perpendicular {200} lattice fringes (d = 0.20 nm) (Figure 1d). The ideal geometrical model is shown in the inset in Figure 1b. The truncated nanocube consists of six {100} facets of truncated squares, twelve {110} facets of rectangles, and eight small {111} facets of hexagons.

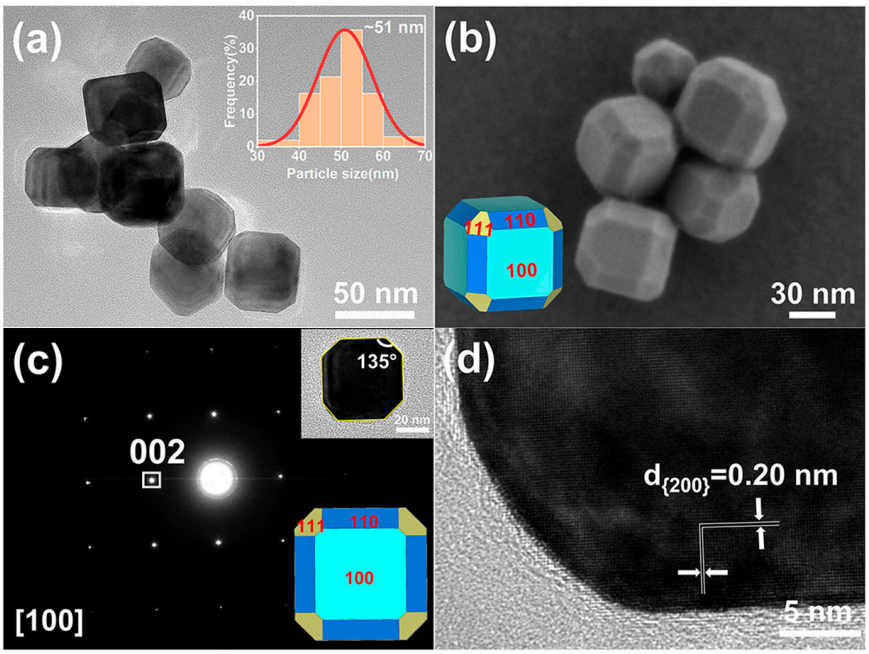


Figure 1. (**a**) TEM, (**b**) FESEM, (**c**) SAED, and (**d**) HRTEM images of the monometallic Pd truncated nanocube ($Pd_{trunc\text{-}cube}$) catalyst. The insets in (**a**–**c**) are particle size distribution, the corresponding geometrical model, and TEM image, respectively.

The bimetallic Pd/Pt truncated nanocube catalysts are named Pd/Pt_x, whose subscript number x represents the actual molar ratio of platinum to palladium in the Pd/Pt nanocrystals measured by the inductively coupled plasma atomic emission spectrometry (ICP-AES). The ICP-AES results reveal that the molar ratios of palladium and platinum contents in all the bimetallic Pd/Pt truncated nanocube catalysts are consistent with the feeding ratios of palladium and platinum during synthesis. This indicates that the added H_2PtCl_6 solution in the synthetic system has been completely reduced.

Figure 2 shows the representative TEM, FESEM, SAED, and HRTEM images of the synthesized bimetallic Pd/Pt truncated nanocube catalysts when the molar ratio of Pt/Pd is below 0.05. It can be seen from the TEM and FESEM images that the $Pd/Pt_{0.005}$ (Figure 2a), $Pd/Pt_{0.01}$ (Figure 2b), $Pd/Pt_{0.015}$ (Figure 2c), $Pd/Pt_{0.02}$ (Figure 2d,e), $Pd/Pt_{0.025}$ (Figure 2h), and $Pd/Pt_{0.05}$ (Figure 2i) nanocrystals exhibit similar truncated nanocube morphologies, which are the same to the shape of the $Pd_{trunc\text{-}cube}$ catalyst. Meanwhile, the results of the particle size distributions show that the average particle sizes of the synthesized bimetallic Pd/Pt nanocrystals are ~51 ± 1 nm, which is the same as the particle size of the $Pd_{trunc\text{-}cube}$ catalyst. It should be noted that the SAED and HRTEM images of the above bimetallic Pd/Pt truncated nanocube catalysts are similar. By taking $Pd/Pt_{0.02}$ as an example, Figure 2f displays the typical SAED pattern of a $Pd/Pt_{0.02}$ truncated nanocube projected along the [100] direction, suggesting that the synthesized Pd/Pt nanocrystals are single crystals. The lattice spacing of the diffraction points marked in the square is 0.20 nm, corresponding to the (200) reflection of fcc Pd. From the HRTEM image (Figure 2g), two sets of perpendicular lattice fringes with lattice spacings of 0.20 nm can be clearly seen over the whole truncated nanocube, further demonstrating the single crystalline nature of the bimetallic $Pd/Pt_{0.02}$ nanocrystals. It can be seen that the lattice spacing of {200} planes in the $Pd/Pt_{0.02}$ catalyst is similar to that of the monometallic $Pd_{trunc\text{-}cube}$ catalyst. This similarity may be attributed to

the low platinum content and the slight difference in lattice parameters between palladium and platinum (a 0.77% difference), resulting in the observed lattice spacing closely matching that of palladium.

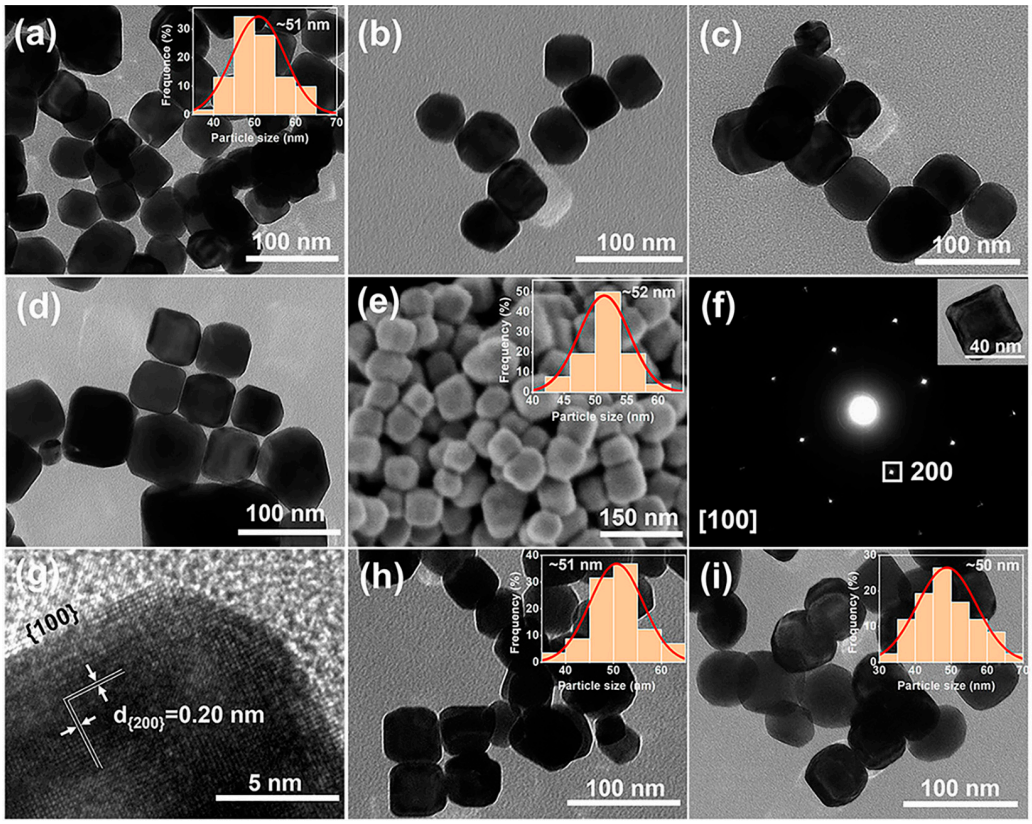


Figure 2. (**a**–**d**,**h**,**i**) TEM, (**e**) FESEM, (**f**) SAED, and (**g**) HRTEM images of the bimetallic Pd/Pt truncated nanocube catalysts. (**a**) $Pd/Pt_{0.005}$, (**b**) $Pd/Pt_{0.01}$, (**c**) $Pd/Pt_{0.015}$, (**d**–**g**) $Pd/Pt_{0.02}$, (**h**) $Pd/Pt_{0.025}$, and (**i**) $Pd/Pt_{0.05}$. The insets are the corresponding particle size distributions and TEM images.

Figure 3 shows the high-angle annular dark field scanning TEM (HAADF-STEM) images and the corresponding energy dispersive X-ray mapping (EDX-mapping) results of the bimetallic $Pd/Pt_{0.005}$, $Pd/Pt_{0.01}$, $Pd/Pt_{0.015}$, $Pd/Pt_{0.02}$, $Pd/Pt_{0.025}$, and $Pd/Pt_{0.05}$ catalysts. All the above bimetallic Pd/Pt catalysts are mainly composed of palladium and platinum, with a small amount of oxygen probably due to the air exposure. It can be seen that platinum is uniformly distributed over the outer surface of the whole bimetallic nanocrystals. According to the edge length and the proportion of crystal facets in $Pd_{trunc\text{-}cube}$ nanocrystals, it can be calculated that the number of atoms on the surface of $Pd_{trunc\text{-}cube}$ nanocrystals is about 1.5% of all atoms in the whole nanocrystal. So when the molar ratio of platinum and palladium is 0.015, the theoretical thickness of platinum atoms on the surface of $Pd_{trunc\text{-}cube}$ nanocrystals is about a single atomic layer. The theoretical thicknesses of platinum formed on the surfaces of the $Pd/Pt_{0.005}$ and $Pd/Pt_{0.01}$ truncated nanocube catalysts are calculated to be 0.3 and 0.7 atomic layers, respectively, which are below one monolayer. The theoretical thicknesses of platinum formed on the surfaces of the $Pd/Pt_{0.02}$, $Pd/Pt_{0.025}$, and $Pd/Pt_{0.05}$ truncated nanocube catalysts are calculated to be 1.3, 1.7, and 3.3 atomic layers, respectively, which are larger than one monolayer.

The line scanning results of $Pd/Pt_{0.02}$, $Pd/Pt_{0.025}$, and $Pd/Pt_{0.05}$ nanocrystals lying flat on the TEM copper grid are shown in Figure 4, where the scanning paths are consistent with the directions of the arrows shown in the HAADF-STEM images. When the scanning direction is along the [100] direction of the fcc metal, as path (1) shown in Figure 4a, the platinum content has a peak on each of the two outer facets of the nanocrystal, which demonstrates that platinum is mainly distributed on the {100} facets of the nanocrystal [15].

When the scanning direction is along the [110] direction of the fcc metal, as path (2) shown in Figure 4a, the distribution of platinum along the scanning path is relatively uniform, and the signal intensity of platinum at the corners is basically the same as that on the crystal facets, indicating that the platinum element is not preferentially deposited at the corners of the nanocrystals. This may be due to the low concentration of the platinum precursor and high reaction temperature in our synthetic process, which leads to a slower atom deposition rate and faster surface diffusion of platinum [7,32]. Consequently, platinum is not deposited at the corners to make the nanocrystals develop into a concave polyhedral structure but is relatively uniformly deposited on the surface of palladium nanocrystals to maintain the shape of the truncated nanocube. When the scanning direction is along the [100] direction, with an increase in the Pt/Pd ratio in the truncated nanocube catalysts, the peak on each of the two outer facets in Pd/$Pt_{0.025}$ and Pd/$Pt_{0.05}$ catalysts gradually increased, indicating an increase in the platinum content on the {100} facets of the Pd/Pt nanocrystals.

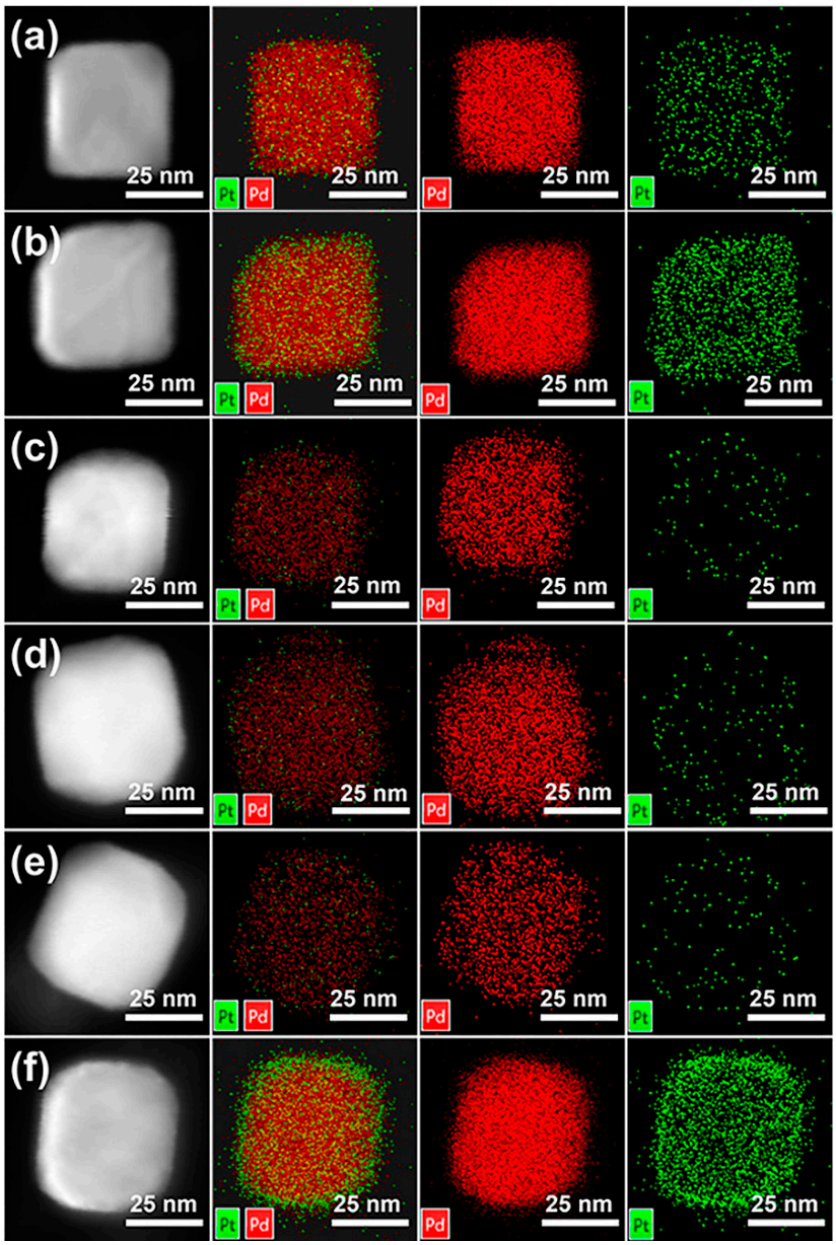


Figure 3. HAADF-STEM images and EDX-mapping results for (**a**) Pd/$Pt_{0.005}$, (**b**) Pd/$Pt_{0.01}$, (**c**) Pd/$Pt_{0.015}$, (**d**) Pd/$Pt_{0.02}$, (**e**) Pd/$Pt_{0.025}$, and (**f**) Pd/$Pt_{0.05}$ bimetallic truncated nanocube catalysts.

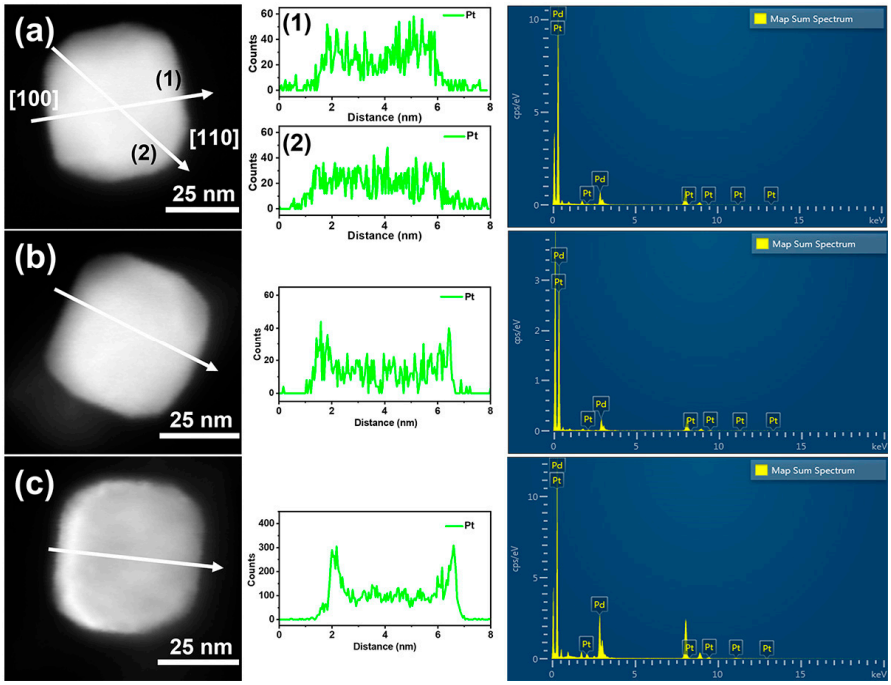


Figure 4. HAADF-STEM images and line scanning results of (**a**) Pd/$Pt_{0.02}$, (**b**) Pd/$Pt_{0.025}$, and (**c**) Pd/$Pt_{0.05}$ truncated nanocube catalysts. The scanning paths are shown in the HAADF-STEM images.

When the amount of H_2PtCl_6 solution added in the synthesis is further increased and the molar ratio between Pt and Pd is larger than 0.1, the TEM and HRTEM images of the synthesized Pd/$Pt_{0.1}$ and Pd/$Pt_{0.2}$ catalysts are shown in Figure 5. From Figure 5a,c, it can be observed that the shapes of the Pd/$Pt_{0.1}$ and Pd/$Pt_{0.2}$ nanocrystals are close to nanocubes at this time, with some small isolated nanoparticles appearing on the surface. The number of small nanoparticles on the Pd/$Pt_{0.2}$ catalyst is significantly larger than that on the Pd/$Pt_{0.1}$ catalyst. The HRTEM images (Figure 5b,d) show that the Pd/$Pt_{0.1}$ and Pd/$Pt_{0.2}$ nanocrystals have discontinuous lattice fringes, indicating that these two catalysts have polycrystalline structures.

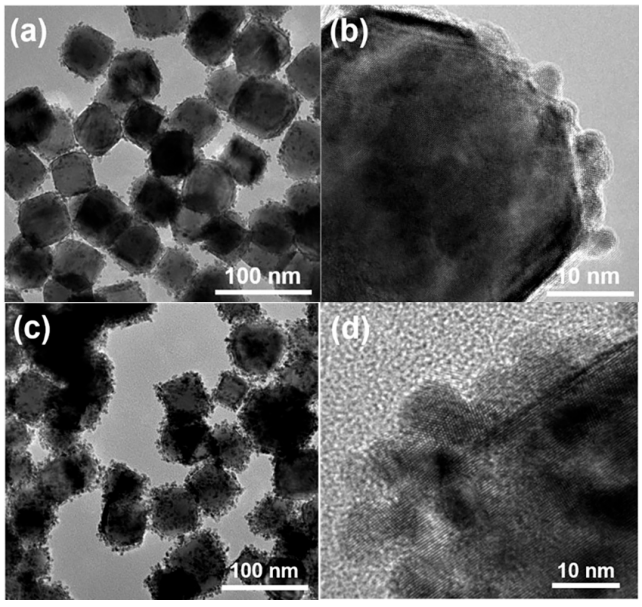


Figure 5. (**a**,**c**) TEM and (**b**,**d**) HRTEM images for Pd/$Pt_{0.1}$ and Pd/$Pt_{0.2}$ catalysts, respectively.

In summary, when the molar ratio of Pt/Pd is ≤0.05, the synthesized nanocrystals ($Pd/Pt_{0.005}$, $Pd/Pt_{0.01}$, $Pd/Pt_{0.015}$, $Pd/Pt_{0.02}$, $Pd/Pt_{0.025}$, and $Pd/Pt_{0.05}$) are single crystalline, which all exhibit truncated nanocube shapes with similar particle sizes and relatively smooth surfaces. When the molar ratio of Pt/Pd is ≥0.1, the synthesized $Pd/Pt_{0.1}$ and $Pd/Pt_{0.2}$ catalysts exhibit polycrystalline structures and nanocube shapes, with many isolated nanoparticles appearing on their surfaces. This may be due to the fact that when the amount of H_2PtCl_6 solution added in the synthetic system is relatively large, the rapid reduction rate of the platinum precursor leads to a high concentration of metallic platinum atoms that quickly form small nanoparticles and thus generate the polycrystalline structure as shown in Figure 5. Nevertheless, when the amount of H_2PtCl_6 solution added in the synthetic system is small, the reduction rate of the platinum precursor is low, and thus metallic platinum is slowly deposited and evenly distributed on the outer surface of the nanocrystals [7,33].

It can be seen from the above research results that $Pd/Pt_{0.005}$, $Pd/Pt_{0.01}$, $Pd/Pt_{0.015}$, $Pd/Pt_{0.02}$, $Pd/Pt_{0.025}$, and $Pd/Pt_{0.05}$ nanocrystals have similar morphologies and particle sizes compared to $Pd_{trunc\text{-}cube}$ nanocrystals. The morphologies and crystal structures of $Pd/Pt_{0.1}$ and $Pd/Pt_{0.2}$ catalysts are different from those of $Pd_{trunc\text{-}cube}$ nanocrystals. Therefore, the crystal structures and electronic properties of $Pd/Pt_{0.005}$, $Pd/Pt_{0.01}$, $Pd/Pt_{0.015}$, $Pd/Pt_{0.02}$, $Pd/Pt_{0.025}$, and $Pd/Pt_{0.05}$ truncated nanocube catalysts were further characterized by X-ray diffraction (XRD) and X-ray photoelectron spectroscopy (XPS) tests.

XRD patterns (Figure 6) of the bimetallic Pd/Pt truncated nanocube catalysts exhibit five characteristic diffraction peaks at 39.9, 46.4, 67.9, 81.9, and 86.4°, which are assigned to the (111), (200), (220), (311), and (222) planes, respectively. Based on the positions of the XRD peaks, the lattice constants of all the bimetallic Pd/Pt nanocrystals are calculated to be 0.391 nm. Therefore, compared to the monometallic Pd catalyst (lattice constant of 0.390 nm), the lattices of the bimetallic Pd/Pt truncated nanocube catalysts expand very slightly.

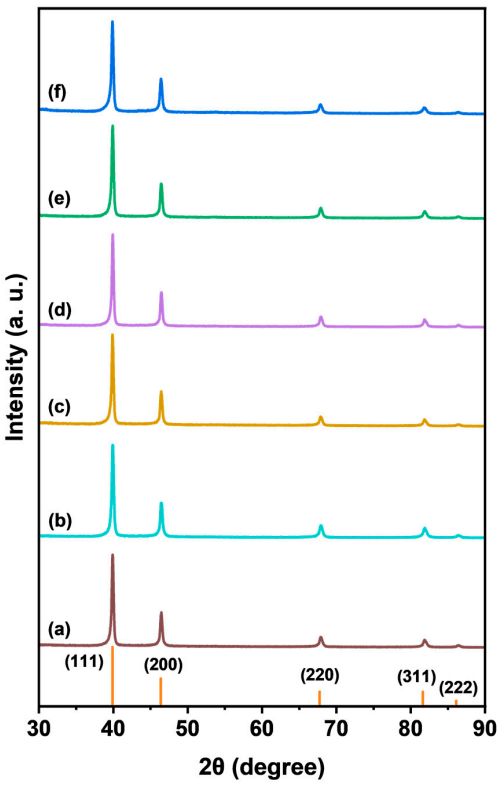


Figure 6. XRD patterns of (a) $Pd/Pt_{0.005}$, (b) $Pd/Pt_{0.01}$, (c) $Pd/Pt_{0.015}$, (d) $Pd/Pt_{0.02}$, (e) $Pd/Pt_{0.025}$, and (f) $Pd/Pt_{0.05}$ catalysts. The vertical bar is the JCPDS card data of monometallic Pd (No. 87-0643).

To study the electronic states of Pd and Pt species in all the bimetallic Pd/Pt catalysts, XPS tests were performed. Figure 7 shows the Pt 4f XPS spectra of all the bimetallic Pd/Pt catalysts. The XPS spectra of platinum in the bimetallic Pd/Pt catalysts are fitted with two peaks with an area ratio of 4:3 and binding energies of 70.9 and 74.2 eV, respectively, which are attributed to the Pt $4f_{7/2}$ and Pt $4f_{5/2}$ peaks, respectively (Table S1). As for the $Pd/Pt_{0.005}$ and $Pd/Pt_{0.01}$ catalysts, their binding energies of Pt $4f_{7/2}$ are slightly lower than that of the standard value (71.0 eV), which may be owing to the partial charge transfer from palladium to platinum [34,35]. With a gradual increase in the platinum content, the binding energy of Pt $4f_{7/2}$ increases from 70.9 eV to 71.1 eV, which is slightly higher than the standard binding energy value of platinum. The binding energy of platinum increases with an increase in the theoretical thickness of the platinum layer, suggesting that the electron-donating effect of palladium gradually weakens with an increase in the platinum thickness, which is consistent with the previously reported results [21]. The contents of platinum in the $Pd/Pt_{0.005}$ and $Pd/Pt_{0.01}$ catalysts are less than one monolayer, so the electron donation from Pd to Pt is the most obvious, resulting in a decrease in the binding energy of platinum compared to the monometallic platinum. In contrast, the theoretical thickness of platinum on the $Pd/Pt_{0.05}$ nanocrystals is 3.3 atomic layers, and therefore it is the least affected by the metal palladium in the nanocrystal. The theoretical thicknesses of platinum on $Pd/Pt_{0.02}$ and $Pd/Pt_{0.025}$ nanocrystals are 1.3 and 1.7 atomic layers, respectively. Thus, the binding energies of Pt $4f_{7/2}$ in $Pd/Pt_{0.02}$ and $Pd/Pt_{0.025}$ catalysts are 71.0 eV, which is located in the middle of 70.9 and 71.1 eV.

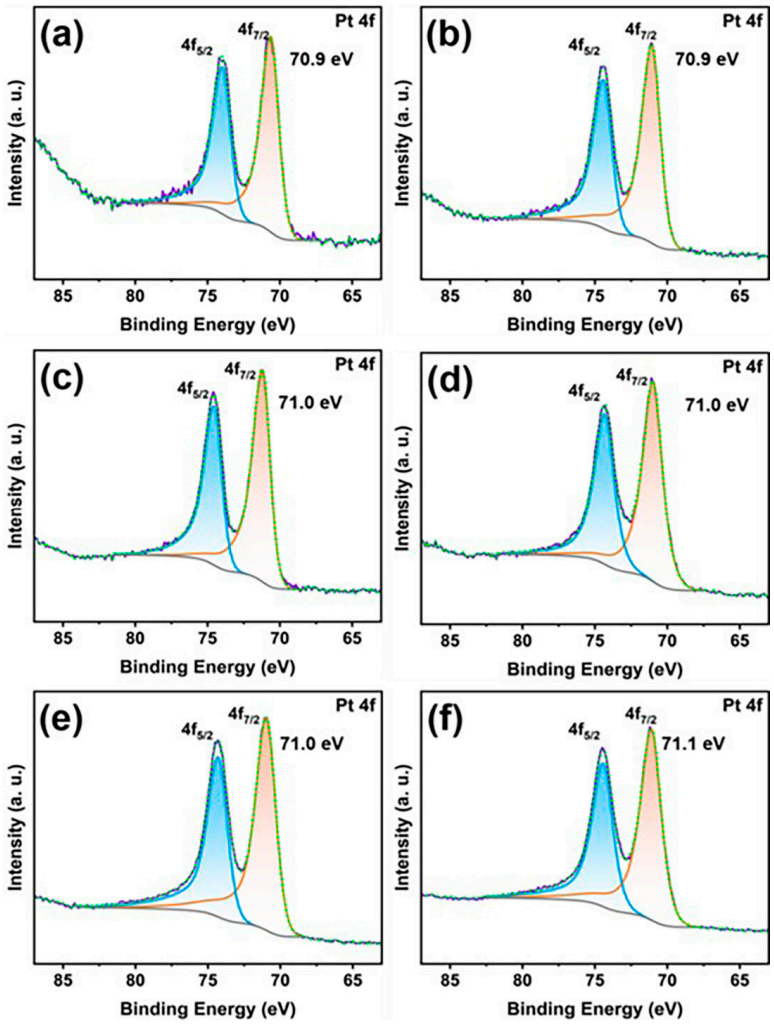


Figure 7. Pt 4f XPS spectra of (**a**) $Pd/Pt_{0.005}$, (**b**) $Pd/Pt_{0.01}$, (**c**) $Pd/Pt_{0.015}$, (**d**) $Pd/Pt_{0.02}$, (**e**) $Pd/Pt_{0.025}$, and (**f**) $Pd/Pt_{0.05}$ catalysts.

The Pd 3d XPS spectra of $Pd/Pt_{0.005}$, $Pd/Pt_{0.01}$, $Pd/Pt_{0.015}$, $Pd/Pt_{0.02}$, $Pd/Pt_{0.025}$, and $Pd/Pt_{0.05}$ catalysts are exhibited in Figure 8. The Pd 3d XPS spectra can be fitted with two main asymmetric peaks, corresponding to the Pd $3d_{5/2}$ and Pd $3d_{3/2}$ peaks of palladium with an area ratio of 3:2 (Table S2). The other two peaks with higher binding energies are attributed to the energy loss peaks of palladium [36,37]. The binding energies of Pd $3d_{5/2}$ in all the bimetallic Pd/Pt catalysts are basically the same (~335.3 eV) and slightly higher than the standard value of metallic palladium (335.1 eV). The increase in palladium binding energy may be ascribed to the transfer of some electrons from palladium to platinum and the inevitable air exposure during the XPS tests [38]. When the molar ratio of Pt/Pd is larger than 0.025 and the theoretical thickness of the platinum layer in Pd/Pt bimetallic nanocrystals is larger than 1.7 atomic layers, another peak with a lower binding energy of 331.7 eV can be observed, which is assigned as the Pt $4d_{3/2}$ peak. When the molar ratio of Pt/Pd is less than 0.02 and the theoretical thickness of the platinum layer is less than 1.3 atomic layers, the peak of Pt $4d_{3/2}$ is not observed. The Pt 4f and Pd 3d XPS spectra demonstrate that the binding energies of palladium in the bimetallic Pd/Pt truncated nanocube catalysts are basically the same, while the binding energies of platinum gradually increase with an increase in the platinum content. This clearly demonstrates that there is an electronic interaction between palladium and platinum in the bimetallic Pd/Pt truncated nanocube catalysts and this electronic effect is closely related to the thickness of the platinum layer.

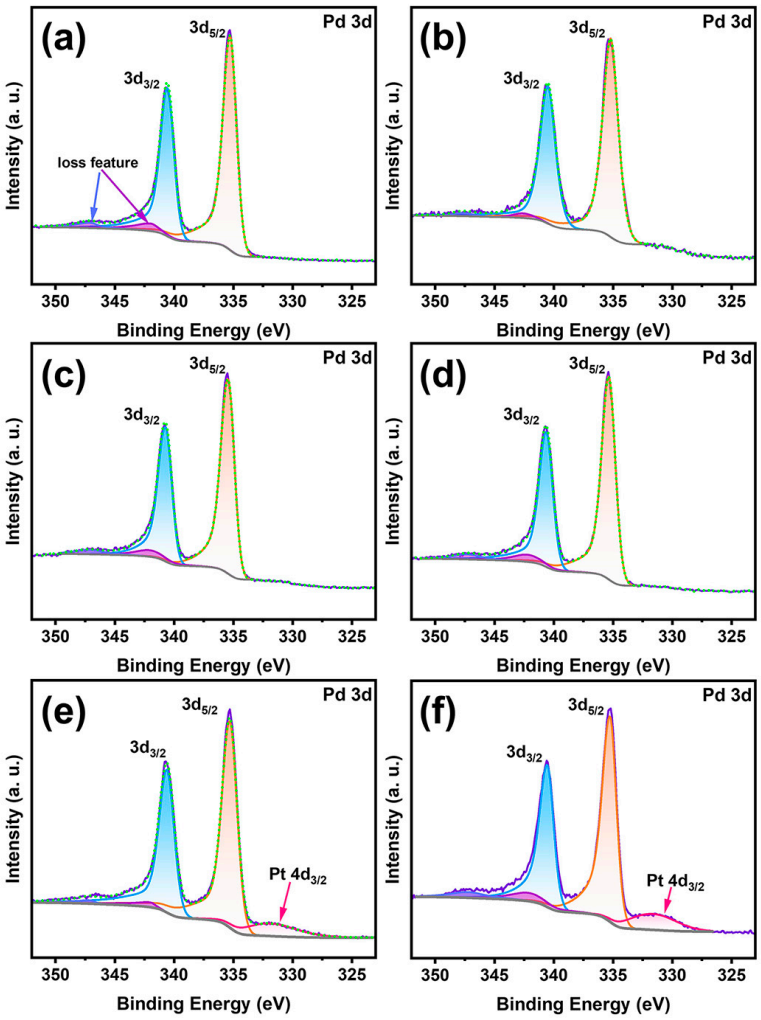


Figure 8. Pd 3d XPS spectra of (**a**) $Pd/Pt_{0.005}$, (**b**) $Pd/Pt_{0.01}$, (**c**) $Pd/Pt_{0.015}$, (**d**) $Pd/Pt_{0.02}$, (**e**) $Pd/Pt_{0.025}$, and (**f**) $Pd/Pt_{0.05}$ catalysts.

2.2. Selective Hydrogenation of Acetophenone

The above-mentioned series of bimetallic Pd/Pt truncated nanocube catalysts with the same morphologies and particle sizes as the $Pd_{trunc\text{-}cube}$ catalyst were selected as model catalysts to study the effect of platinum addition and the dependence of platinum content on the catalytic performance in the selective hydrogenation of acetophenone. For comparison, we also tested the catalytic performance of monometallic Pd and Pt catalysts in the selective hydrogenation of acetophenone under the same reaction conditions. Figure 9 shows the conversion of acetophenone as a function of reaction time on $Pd/Pt_{0.005}$, $Pd/Pt_{0.01}$, $Pd/Pt_{0.015}$, $Pd/Pt_{0.02}$, $Pd/Pt_{0.025}$, and $Pd/Pt_{0.05}$ truncated nanocube catalysts. It can be clearly observed from Figure 9 that the addition of platinum is beneficial to improving the catalytic activity of the Pd nanocrystal catalyst. With an increase in the theoretical thickness of the platinum layer on the surface of the bimetallic Pd/Pt catalysts, the activity of the catalyst increases first, reaches the maximum with the Pt/Pd molar ratios of 0.02~0.025 and the Pt theoretical thicknesses of 1.3~1.7 atomic layers, and then decreases.

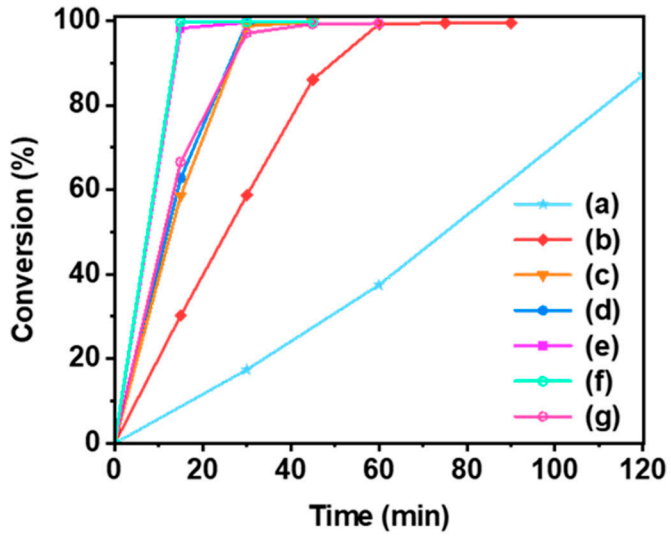


Figure 9. Conversion of acetophenone as a function of reaction time, (a) $Pd_{trunc\text{-}cube}$, (b) $Pd/Pt_{0.005}$, (c) $Pd/Pt_{0.01}$, (d) $Pd/Pt_{0.015}$, (e) $Pd/Pt_{0.02}$, (f) $Pd/Pt_{0.025}$, and (g) $Pd/Pt_{0.05}$ catalysts. Reaction conditions: 4 mg of catalyst, 17 mL of methanol, 20 μL of acetophenone, 288 K, atmospheric pressure, hydrogen flow rate 60 $mL{\cdot}min^{-1}$.

Table 1 lists the reaction rates on the above bimetallic Pd/Pt truncated nanocube catalysts with different platinum contents in the selective hydrogenation of acetophenone. For comparison, the reaction rates on monometallic Pd and Pt catalysts are also shown. The reaction rate of the $Pd/Pt_{0.005}$ catalyst is 49.4 $mmol{\cdot}h^{-1}{\cdot}g_{cat.}{}^{-1}$, which is 3.7 times that of the monometallic $Pd_{trunc\text{-}cube}$ catalyst. With an increase in the platinum content, the reaction rates of $Pd/Pt_{0.01}$ and $Pd/Pt_{0.015}$ catalysts are increased to 97.7 and 104 $mmol{\cdot}h^{-1}{\cdot}g_{cat.}{}^{-1}$, respectively, which are much higher than that on the $Pd/Pt_{0.005}$ catalyst. With a further increase in the platinum content, the catalytic activity of $Pd/Pt_{0.02}$ and $Pd/Pt_{0.025}$ catalysts increase rapidly, and the acetophenone hydrogenation reaction is basically completed within 15 min. The reaction rates on $Pd/Pt_{0.02}$ and $Pd/Pt_{0.025}$ catalysts are ca. 12 times higher than that on $Pd_{trunc\text{-}cube}$ catalyst. It should be noted that under the current reaction conditions (the usage of 20 μL acetophenone), the hydrogenation reactions on $Pd/Pt_{0.02}$ and $Pd/Pt_{0.025}$ catalysts are too fast to sample at intervals. Thus, the calculated reaction rates are not accurate enough and will be redetermined and compared later in the following texts. As the molar ratio of platinum to palladium was further increased to 0.05, the activity of the $Pd/Pt_{0.05}$ catalyst diminished compared to the $Pd/Pt_{0.02}$ and $Pd/Pt_{0.025}$ catalysts. However, the activity of the $Pd/Pt_{0.05}$ catalyst is still 7.6 times higher than that of the monometallic $Pd_{trunc\text{-}cube}$ catalyst. Compared with monometallic Pd and Pt catalysts, the

activities of the bimetallic Pd/Pt catalysts are generally higher, which may be due to the stress generated by the lattice mismatches and the electronic interaction between platinum and palladium in the bimetallic Pd/Pt catalysts [39], in accordance with our XPS results.

Table 1. Reaction rates on bimetallic Pd/Pt, monometallic Pd, and monometallic Pt catalysts in the selective hydrogenation of acetophenone.

Catalyst	Reaction Rate ($mmol \cdot h^{-1} \cdot g_{cat.}{}^{-1}$)
$Pd_{trunc\text{-}cube}$	13.5
$Pd/Pt_{0.005}$	49.4
$Pd/Pt_{0.01}$	97.7
$Pd/Pt_{0.015}$	104
$Pd/Pt_{0.02}$ *	161
$Pd/Pt_{0.025}$ *	162
$Pd/Pt_{0.05}$	103
Pt	14.1

Reaction conditions: 4 mg of catalyst, 17 mL of methanol, 20 µL of acetophenone, 288 K, atmospheric pressure, hydrogen flow rate of 60 mL min^{-1}. The two catalysts marked with "*" have reactions that are too fast under current conditions, making it difficult to sample at intervals and measure accurate reaction rates. These two reaction rates will be redetermined and compared in the following text.

In all the bimetallic Pd/Pt truncated nanocube catalysts in the selective hydrogenation of acetophenone, during the initial stage of the reaction, the yield of 1-phenylethanol increases as acetophenone is consumed. As the reaction time is further prolonged, the yield of 1-phenylethanol reaches its maximum value, and then gradually decreases with the aimed-for product 1-phenylethnaol, which is gradually transformed into other by-products. Therefore, we measured the distribution of the aimed-for product 1-phenylethanol and various possible by-products when the yield of 1-phenylethanol reached its maximum to better study the carbonyl selectivity of the bimetallic Pd/Pt catalysts. Table 2 presents the product distribution at the maximum yield of 1-phenylethanol on bimetallic Pd/Pt, monometallic Pd, and monometallic Pt catalysts. The conversion of acetophenone and the corresponding reaction time when the yield of 1-phenylethanol reaches its maximum are also shown in Table 2. The experimental results demonstrate that, for the $Pd_{trunc\text{-}cube}$ catalyst, the maximum yield of the target product, 1-phenylethanol (PE), is 90.6%, with ethylbenzene (EB) being the sole by-product with a yield of 5.8%. As the platinum content gradually increases in the $Pd/Pt_{0.005}$, $Pd/Pt_{0.01}$, $Pd/Pt_{0.015}$, and $Pd/Pt_{0.02}$ catalysts, the selectivities of these catalysts for 1-phenylethanol are increased to ~97%. Evidently, the Pd/Pt truncated nanocube catalyst with an appropriate Pd/Pt molar ratio exhibits superior selectivity for 1-phenylethanol compared to the monometallic $Pd_{trunc\text{-}cube}$ counterpart. As the platinum content is further increased, the selectivities of $Pd/Pt_{0.025}$ and $Pd/Pt_{0.05}$ catalysts for 1-phenylethanol decreased by 4.8% and 8.3%, respectively, compared to the $Pd/Pt_{0.02}$ catalyst. On the $Pd/Pt_{0.05}$ catalyst, the selectivity of 1-phenylethanol is 4.5% lower than that on the $Pd_{trunc\text{-}cube}$ catalyst, while the by-products such as acetylcyclohexane (AC), 1-cyclohexylethanol (CE), and ethylcyclohexane (EC) increased significantly. This clearly demonstrates that the introduction of excess platinum in the bimetallic Pd/Pt truncated nanocube catalysts actually reduces the selectivity for 1-phenylethanol. As for the monometallic Pt catalyst, the selectivity for 1-phenylethanol is only 80.8%. It can be clearly seen that the selectivities of bimetallic Pd/Pt catalysts are much better than those of monometallic Pt catalysts. Literature reports indicate that in the selective hydrogenation of acetophenone, monometallic Pd catalysts mainly catalyze the formation of EB as the main by-product while monometallic Pt catalysts usually catalyze the formation of various kinds of by-products, such as EB, AC, CE, and EC [40,41]. Therefore, as the molar ratio of Pt/Pd is larger than 0.05, the catalytic behavior of the bimetallic Pd/Pt truncated nanocube catalyst becomes more similar to that of the monometallic Pt catalyst and the carbonyl selectivity decreases.

Table 2. Product distribution at maximum yield of 1-phenylethanol on bimetallic Pd/Pt, monometallic Pd, and monometallic Pt catalysts.

Catalyst	Reaction Time (min)	Conversion (%)	Product Selectivity (%)				
			PE	EB	AC	CE	EC
$Pd_{trunc\text{-}cube}$	180	96.4	94.0	6.0	0	0	0
$Pd/Pt_{0.005}$	60	99.5	96.9	3.0	0.1	0	0
$Pd/Pt_{0.01}$	45	99.6	96.7	3.0	0.3	0	0
$Pd/Pt_{0.015}$	30	99.6	97.2	2.3	0.3	0.1	0
$Pd/Pt_{0.02}$	15	98.3	97.8	1.7	0.5	0	0
$Pd/Pt_{0.025}$	15	99.7	93.0	6.2	0.4	0.3	0.04
$Pd/Pt_{0.05}$	30	99.5	89.5	5.0	3.4	1.2	0.8
Pt	180	99.6	80.8	6.0	5.8	5.0	2.3

Reaction conditions: 4 mg of catalyst, 17 mL of methanol, 20 μL of acetophenone, 288 K, atmospheric pressure, hydrogen flow rate of 60 $mL \cdot min^{-1}$. PE, EB, AC, CE, and EC represent 1-phenylethanol, ethylbenzene, acetylcyclohexane, 1-cyclohexylethanol, and ethylcyclohexane, respectively.

As addressed in the discussion of Table 1, when using 20 μL of acetophenone as the reactant, the reactions on the $Pd/Pt_{0.02}$ and $Pd/Pt_{0.025}$ catalysts are so fast that it is difficult to obtain accurate reaction rates. Our previous experimental results show that the liquid-phase hydrogenation of acetophenone is zero-order dependent regarding acetophenone [30,31]. The reaction order of H_2 for the selective hydrogenation of acetophenone over $Pd/Pt_{0.02}$ and $Pd/Pt_{0.025}$ catalysts is first-order. Therefore, we tentatively increased the dosage of acetophenone to 25 times the original amount (from 20 μL to 500 μL), while keeping other reaction conditions unchanged, in order to obtain more accurate reaction rates on the $Pd/Pt_{0.02}$ and $Pd/Pt_{0.025}$ catalysts in the selective hydrogenation of acetophenone. The evolution of the yield of 1-phenylethanol in the selective hydrogenation of acetophenone over $Pd/Pt_{0.025}$ and $Pd/Pt_{0.02}$ catalysts as a function of reaction time when using 500 μL of acetophenone is shown in Figure 10. The reaction rates of the acetophenone hydrogenation reaction on $Pd/Pt_{0.02}$ and $Pd/Pt_{0.025}$ catalysts are 1.07×10^3 and 760 $mmol \cdot h^{-1} \cdot g_{cat.}{}^{-1}$, respectively, indicating that the $Pd/Pt_{0.02}$ catalyst has a much higher level of activity. Therefore, among all the bimetallic Pd/Pt truncated nanocube catalysts, the $Pd/Pt_{0.02}$ catalyst exhibits the highest activity. The reaction rate of the $Pd/Pt_{0.02}$ catalyst is 79 and 76 times higher than that of monometallic Pd and Pt catalysts. The maximum yield of 1-phenylethanol on $Pd/Pt_{0.02}$ catalyst when using 500 μL of acetophenone is 97.2%, with ethylbenzene being the main by-product with a yield of 2.5%. The total yield of the other three by-products (AC, CE, and EC) is below 0.2%. Compared to the $Pd/Pt_{0.02}$ catalyst, the activity of the $Pd/Pt_{0.025}$ catalyst decreases by 29%. The theoretical thicknesses of the Pt layers in $Pd/Pt_{0.02}$ and $Pd/Pt_{0.025}$ catalysts are 1.3 and 1.7 atomic layers, respectively. Compared with the $Pd/Pt_{0.02}$ catalyst, the theoretical thickness of platinum in the $Pd/Pt_{0.025}$ catalyst only increases by 0.4 atomic layers, but the hydrogenation activity decreases by 29%. This further demonstrates that the electronic interaction between palladium and platinum in the Pd/Pt bimetallic nanocrystal catalysts is closely related to the molar ratio between platinum and palladium and the resulting thickness of the platinum layer on the Pd nanocrystals [15,42]. When the theoretical thickness of Pt is 1.3 atomic layers, the activity of the bimetallic Pd/Pt truncated nanocube catalyst in the selective hydrogenation of acetophenone reaches its maximum.

It can be concluded that the $Pd/Pt_{0.02}$ catalyst with a full Pt coverage closest to one monolayer exhibits the highest level of mass activity among the bimetallic Pd/Pt truncated nanocube catalysts. Our finding is in accordance with the literature reports [15,17]. Zhang and co-workers studied the shell thickness-dependent catalytic performance of Pd@Pt core–shell octahedral nanoparticles for p-chloronitrobenzene hydrogenation and found that the Pd@Pt octahedral nanoparticles with one atomic Pt layer demonstrated the best catalytic activity [15]. Cao and co-workers studied the shell-thickness effect of Pd@Pt core–shell nanoparticles towards the preferential oxidation of CO in the presence of excess H_2 and also found that the catalyst with a monolayer Pt shell showed optimal performance [17].

The enhanced catalytic performance of the $Pd/Pt_{0.02}$ catalyst possibly originates from the optimal interaction between the surface Pt monolayer and the Pd subsurface layer, which adjusts the d-band center and the electronic state of surface Pt atoms to be suitable for the selective hydrogenation of acetophenone [4,15,17,43].

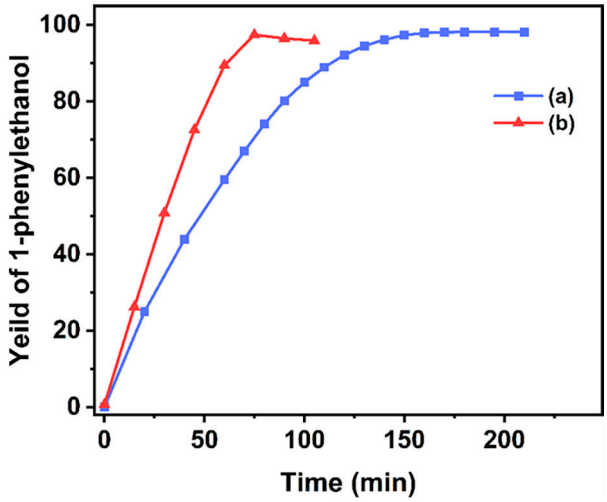


Figure 10. (a) The yield of 1-phenylethanol in the selective hydrogenation of acetophenone over $Pd/Pt_{0.025}$ and (b) $Pd/Pt_{0.02}$ catalysts as a function of reaction time. Reaction conditions: 4 mg of catalyst, 17 mL of methanol, 500 μL of acetophenone, reaction temperature 288 K, hydrogen flow rate 60 $mL \cdot min^{-1}$.

3. Materials and Methods

3.1. Materials

Palladium chloride was obtained from J&K Scientific Ltd. (Beijing, China). Chloroplatinate hexahydrate was obtained from Sigma-Aldrich (St. Louis, MO, USA). L-ascorbic acid, hydro-chloric acid, acetophenone, and methanol were obtained from Sino-pharm Chemical Reagent Co., Ltd. (Shanghai, China). All chemicals were utilized as received and not further purified.

3.2. Catalyst Preparation

Synthesis of bimetallic Pd/Pt truncated nanocube catalysts: Pd/Pt truncated nanocubes were synthesized in a three-neck flask under flowing N_2 (50 $mL \cdot min^{-1}$). Briefly, 5 mL of H_2PdCl_4 solution (10 mM, pH = 0.9) was added into a 250 mL three-neck flask, followed by the addition of 100 mL of deionized water. After placing the reaction system in an oil bath for 30 min with the temperature of the reaction mixture kept at 368 K, 0.5 mL of ascorbic acid solution (0.1 M) was added into the reaction mixture at one time with a pipette, and the reaction lasted for 2 h. Then, a certain amount (25, 50, 75, 100, 125, 250, 500, and 1000 μL) of H_2PtCl_6 solution (10 mM, pH = 0.9) was added at a rate of 19.3 $\mu L \cdot min^{-1}$ with a peristaltic pump, and the reaction continued for another 1 h after H_2PtCl_6 was completely added to the synthetic system. The synthesized catalysts were named $Pd/Pt_{0.005}$, $Pd/Pt_{0.01}$, $Pd/Pt_{0.015}$, $Pd/Pt_{0.02}$, $Pd/Pt_{0.025}$, $Pd/Pt_{0.05}$, $Pd/Pt_{0.1}$, and $Pd/Pt_{0.2}$, respectively, whose subscript numbers represent the actual molar ratios of platinum to palladium in the Pd/Pt nanocrystals measured by ICP-AES. After the synthesis, the obtained nanocrystals were centrifuged, washed three times with deionized water, washed three times with methanol, and then dispersed in methanol by ultrasonic for activity tests.

Synthesis of monometallic Pd truncated nanocube catalyst: The monometallic Pd truncated nanocube catalyst (denoted as $Pd_{trunc\text{-}cube}$) was synthesized according to the synthetic process reported in our previous work [31].

Synthesis of monometallic Pt nanocrystal catalyst: The synthesis of monometallic Pt catalyst was similar to the Pd/Pt bimetallic nanocrystal. An amount of 5 mL of H_2PtCl_6

solution (10 mM, pH = 0.9) and 100 mL of deionized water were mixed in the reaction system, and then 2 mL of ascorbic acid solution (0.1 M) was added at one time with a pipette. The reaction lasted for 3 h, and the synthesized Pt nanocrystal catalyst was centrifuged and dispersed in methanol for the activity test.

3.3. Catalyst Characterization

Transmission electron microscope (TEM) images were collected on an HT7700 Exalens electron microscope (Hitachi, Tokyo, Japan) operated at 120 kV. The Pd and Pt content of the catalysts were determined by inductively coupled plasma atomic emission spectrometry (ICP-AES) using the 725-ES plasma emission spectrometer (Varian, Palo Alto, CA, USA). Field-emission scanning electron microscopic (FESEM) images were obtained on a SU8600 or S-4800 electron microscope (Hitachi, Tokyo, Japan). Energy dispersive X-ray mapping (EDX-mapping) analyses, selected-area electron diffraction (SAED) patterns, high-resolution TEM (HRTEM) images, and the high-angle annular dark field scanning TEM (HAADF-STEM) images were acquired on a field-emission transmission electron microscope (FEI, Tecnai G2 F20 S-Twin, Hillsboro, OR, USA). The powder X-ray diffraction (XRD) patterns were recorded using Cu-Kα source (λ = 0.15418 nm) on a D2 PHASER X-ray diffractometer (Bruker, Karlsruhe, Germany). The X-ray photoelectron spectroscopy (XPS) analysis was performed on Axis Ultra DLD system (Kratos, Manchester, UK) using Al Kα (1486.6 eV) X-ray source. The charge effect on the catalyst surface was corrected using surface contamination carbon (C1s = 284.6 eV) as the internal standard.

3.4. Activity Test

Liquid phase selective hydrogenation of acetophenone: 17 mL of methanol and fresh catalyst (4 mg) were added to a 100 mL three-neck flask at 288 K, and atmospheric high-purity nitrogen was introduced into the flask, followed by high-purity hydrogen at a rate of 60 mL·min^{-1} to replace the nitrogen in the flask. After adding acetophenone (20 µL or 500 µL), turn on stirring at 1000 rpm, and take samples intermittently during the reaction. The reaction sample was subjected to high-speed centrifugation to remove the catalyst, and then the supernatant was taken for chromatographic analysis.

4. Conclusions

A series of bimetallic Pd/Pt truncated nanocube catalysts with different Pt/Pd ratios were successfully synthesized by a colloidal method without using any capping agents. It was found that when the molar ratio of platinum to palladium is below 0.05, the resulting bimetallic Pd/Pt truncated nanocube catalysts are single crystals with relatively smooth surfaces. The morphologies and particle sizes of the bimetallic Pd/Pt catalysts are similar to those of the monometallic Pd truncated nanocube catalyst. In contrast, when the Pt/Pd molar ratio is larger than 0.1, small isolated Pt nanoparticles emerge on the surface of Pd nanocrystals, and the resulting Pd/Pt nanocrystals are polycrystalline. Consequently, we employed the single crystalline bimetallic Pd/Pt truncated nanocubes with the same morphologies and sizes as model catalysts to investigate the dependence of Pt thickness on the catalytic performance in the selective hydrogenation of acetophenone. It was found that the deposition of Pt notably boosts the activity of the Pd truncated nanocube catalyst. As the Pt content increases, both the activity of the Pd/Pt catalysts and the selectivity for 1-phenylethanol exhibit an initial increase, reach a maximum when the theoretical thickness of Pt is 1.3 atomic layers, and then decrease, even with a slight increase in Pt thickness of 0.4 atomic layers. Notably, the Pd/$Pt_{0.02}$ catalyst demonstrates the highest catalytic activity, achieving an acetophenone hydrogenation rate of 1.07 $\times$ 10^3 mmol·h^{-1}·$g_{cat.}{}^{-1}$, which is 79 and 75 times higher than that of the monometallic Pd and Pt catalysts. The maximum yield of 1-phenylethanol on the bimetallic Pd/$Pt_{0.02}$ catalyst reaches 97.2%, indicating a 6.6% and 16.7% improvement over the monometallic Pd and Pt catalysts, respectively.

Supplementary Materials: The following supporting information can be downloaded at https://www.mdpi.com/article/10.3390/catal14120900/s1, Table S1: Deconvolution of Pt 4f XPS spectra of the bimetallic Pd/Pt truncated nanocube catalysts; Table S2: Deconvolution of Pd 3d XPS spectra of the bimetallic Pd/Pt truncated nanocube catalysts.

Author Contributions: Conceptualization, X.C. and X.Y.; methodology, X.Y.; validation, J.B. and J.C.; investigation, X.Y.; data curation, X.Y., J.B. and J.C.; writing—original draft preparation, J.B. and X.Y.; writing—review and editing, X.C. and H.H.; supervision, X.C., B.Y. and H.H.; project administration, X.C. and H.H.; funding acquisition, X.C. All authors have read and agreed to the published version of the manuscript.

Funding: This work was supported by the National Natural Science Foundation of China (22172035) and the National Key Research and Development Program of China (2023YFA1507602).

Data Availability Statement: Data are contained within the article and Supplementary Materials.

Conflicts of Interest: The authors declare no conflicts of interest.

References

1. Wu, W.Y.; Wu, S.; Tjiu, W.W.; Tan, H.R.; Leong, F.Y.; Lim, P.C.; Wang, S.; Jiang, W.; Ji, R.; Zhu, Q.; et al. Oxygen plasma induced nanochannels for creating bimetallic hollow nanocrystals. *ACS Nano* **2023**, *17*, 17536–17544. [CrossRef] [PubMed]
2. Kang, Y.J.; Ye, X.C.; Chen, J.; Cai, Y.; Diaz, R.E.; Adzic, R.R.; Stach, E.A.; Murray, C.B. Design of Pt-Pd binary superlattices exploiting shape effects and synergistic effects for oxygen reduction reactions. *J. Am. Chem. Soc.* **2012**, *135*, 42–45. [CrossRef]
3. Lim, B.; Jiang, M.; Yu, T.; Camargo, P.H.C.; Xia, Y. Nucleation and growth mechanisms for Pd-Pt bimetallic nanodendrites and their electrocatalytic properties. *Nano Res.* **2010**, *3*, 69–80. [CrossRef]
4. Zhang, J.L.; Vukmirovic, M.B.; Xu, Y.; Mavrikakis, M.; Adzic, R.R. Controlling the catalytic activity of platinum-monolayer electrocatalysts for oxygen reduction with different substrates. *Angew. Chem. Int. Ed.* **2005**, *44*, 2132–2135. [CrossRef]
5. Bueno, S.L.A.; Zhan, X.; Wolfe, J.; Chatterjee, K.; Skrabalak, S.E. Phase-controlled synthesis of Pd-Sn nanocrystal catalysts of defined size and shape. *ACS Appl. Mater. Interfaces* **2021**, *13*, 51876–51885. [CrossRef] [PubMed]
6. Zhu, J.W.; Elnabawy, A.O.; Lyu, Z.H.; Xie, M.H.; Murray, E.A.; Chen, Z.T.; Jin, W.Q.; Mavrikakis, M.; Xia, Y.N. Facet-controlled Pt-Ir nanocrystals with substantially enhanced activity and durability towards oxygen reduction. *Mater. Today* **2020**, *35*, 69–77. [CrossRef]
7. Gao, W.P.; Elnabawy, A.O.; Hood, Z.D.; Shi, Y.F.; Wang, X.; Roling, L.T.; Pan, X.Q.; Mavrikakis, M.; Xia, Y.N.; Chi, M.F. Atomistic insights into the nucleation and growth of platinum on palladium nanocrystals. *Nat. Commun.* **2021**, *12*, 3215. [CrossRef]
8. Chung, D.Y.; Jun, S.W.; Yoon, G.; Kwon, S.G.; Shin, D.Y.; Seo, P.; Yoo, J.M.; Shin, H.; Chung, Y.H.; Kim, H.; et al. Highly durable and active PtFe nanocatalyst for electrochemical oxygen reduction reaction. *J. Am. Chem. Soc.* **2015**, *137*, 15478–15485. [CrossRef]
9. Zhang, J.L.; Vukmirovic, M.B.; Sasaki, K.; Nilekar, A.U.; Mavrikakis, M.; Adzic, R.R. Mixed-metal Pt monolayer electrocatalysts for enhanced oxygen reduction kinetics. *J. Am. Chem. Soc.* **2005**, *127*, 12480–12481. [CrossRef]
10. Wang, R.; He, H.; Wang, J.N.; Liu, L.C.; Dai, H.X. Shape-regulation: An effective way to control CO oxidation activity over noble metal catalysts. *Catal. Today* **2013**, *201*, 68–78. [CrossRef]
11. Xu, Q.F.; Chen, W.L.; Yan, Y.C.; Wu, Z.M.; Jiang, Y.; Li, J.J.; Bian, T.; Zhang, H.; Wu, J.B.; Yang, D.R. Multimetallic AuPd@Pd@Pt core-interlayer-shell icosahedral electrocatalysts for highly efficient oxygen reduction reaction. *Sci. Bull.* **2018**, *63*, 494–501. [CrossRef] [PubMed]
12. Li, L.; Ye, X.T.; Xiao, Q.; Zhu, Q.Y.; Hu, Y.; Han, M.J. Nanostructure engineering of Pt/Pd-based oxygen reduction reaction electrocatalysts. *Phys. Chem. Chem. Phys.* **2023**, *25*, 30172–30187. [CrossRef] [PubMed]
13. Han, Y.J.; Kim, J.; Lee, S.U.; Choi, S.I.; Hong, J.W. Synthesis of Pd-Pt ultrathin assembled nanosheets as highly efficient electrocatalysts for ethanol oxidation. *Chem. Asian J.* **2020**, *15*, 1324–1329. [CrossRef]
14. Kim, M.C.; Han, G.H.; Xiao, X.Y.; Song, J.; Hong, J.; Jung, E.; Kim, H.K.; Ahn, J.P.; Han, S.S.; Lee, K.Y.; et al. Anisotropic growth of Pt on Pd nanocube promotes direct synthesis of hydrogen peroxide. *Appl. Surf. Sci.* **2021**, *562*, 150031. [CrossRef]
15. Zhang, P.P.; Hu, Y.B.; Li, B.H.; Zhang, Q.J.; Zhou, C.; Yu, H.B.; Zhang, X.J.; Chen, L.; Eichhorn, B.; Zhou, S.H. Kinetically stabilized Pd@Pt core-shell octahedral nanoparticles with thin Pt layers for enhanced catalytic hydrogenation performance. *ACS Catal.* **2015**, *5*, 1335–1343. [CrossRef]
16. Lin, Y.F.; Tian, N.; Xiao, C.; Sheng, T.; Li, G.; Zhang, F.Y.; Ye, J.-Y.; Xu, B.B.; Zhou, Z.Y.; Sun, S.G. Effects of atom arrangement and thickness of Pt atomic layers on Pd nanocrystals for electrocatalysis. *Electrochim. Acta* **2018**, *271*, 519–525. [CrossRef]
17. Cao, K.; Liu, X.; Zhu, Q.Q.; Shan, B.; Chen, R. Atomically Controllable Pd@Pt Core-Shell Nanoparticles towards Preferential Oxidation of CO in Hydrogen Reactions Modulated by Platinum Shell Thickness. *ChemCatChem* **2015**, *8*, 326–330. [CrossRef]
18. Chen, S.; Zhao, J.K.; Su, H.Y.; Li, H.L.; Wang, H.L.; Hu, Z.P.; Bao, J.; Zeng, J. Pd-Pt tesseracts for the oxygen reduction reaction. *J. Am. Chem. Soc.* **2021**, *143*, 496–503. [CrossRef]
19. Wang, T.P.; Hong, B.D.; Lin, Y.-M.; Lee, C.L. Catalysis of the d-glucose oxidation reaction using octahedral, rhombic dodecahedral, and cubic Pd@Pt core-shell nanoparticles. *Appl. Catal. B Environ.* **2020**, *260*, 118140. [CrossRef]

20. Zhang, Y.; Bu, L.Z.; Jiang, K.Z.; Guo, S.J.; Huang, X.Q. Concave Pd-Pt core-shell nanocrystals with ultrathin Pt shell feature and enhanced catalytic performance. *Small* **2015**, *12*, 706–712. [CrossRef]
21. Hashiguchi, Y.; Nakamura, I.; Honma, T.; Matsushita, T.; Murayama, H.; Tokunaga, M.; Choe, Y.K.; Fujitani, T. Effects of the Pt shell thickness on the oxygen reduction reaction on a well-defined Pd@Pt core-shell model surface. *ChemPhysChem* **2023**, *24*, e202200389. [CrossRef] [PubMed]
22. Li, X.L.; Li, B.Z.; Cheng, M.H.; Du, Y.K.; Wang, X.M.; Yang, P. Catalytic hydrogenation of phenyl aldehydes using bimetallic Pt/Pd and Pt/Au nanoparticles stabilized by cubic silsesquioxanes. *J. Mol. Catal. A Chem.* **2008**, *284*, 1–7. [CrossRef]
23. Cui, T.Y.; Ling, Y.; Meng, J.P.; Li, K.; Liang, C.H.; Li, C. Enhanced catalytic performance of Pd-Pt bimetallic alloy nanocatalyst for hydrogenation of nitrile butadiene rubber. *Mol. Catal.* **2023**, *545*, 113163. [CrossRef]
24. Mojica Sepúlveda, R.D.; Mendoza Herrera, L.J.; Vetere, V.; Soria, D.B.; Grumel, E.E.; Cabello, C.I.; Trivi, M.; Tebaldi, M.C. Influence of physicochemical properties of Ni/clinoptilolite catalysts in the hydrogenation of acetophenone. *ACS Omega* **2023**, *8*, 4727–4735. [CrossRef] [PubMed]
25. Guo, G.H.; Zhang, Y.; Zhang, H.; Zhang, X.C.; He, X.H.; Ji, H.B. Selective hydrogenation of aromatic ketone to aromatic alcohol over Pd single-atom catalysts. *Ind. Eng. Chem. Res.* **2023**, *62*, 19585–19591. [CrossRef]
26. Lin, S.; Liu, J.; Ma, L. Ni@C catalyzed hydrogenation of acetophenone to phenylethanol under industrial mild conditions in a flow reactor. *React. Chem. Eng.* **2022**, *7*, 1126–1135. [CrossRef]
27. Gou, Y.; Liang, X.; Chen, B.H. Catalytic hydrogenation of acetophenone over shape controlled Pd catalysts supported on sheet-like NiO. *Catal. Today* **2013**, *216*, 200–204. [CrossRef]
28. Zhang, X.B.; Lu, W.N.; Wang, J.L.; Liao, B.H.; Qin, Y.H.; Zhang, Y.J.; Zhang, B.; Xin, S.A. Selective catalytic hydrogenation of acetophenone to1-phenylethanolover Co/mordenite in water. *Catal. Commun.* **2019**, *119*, 124–128. [CrossRef]
29. Costa, D.C.; Soldati, A.L.; Pecchi, G.; Bengoa, J.F.; Marchetti, S.G.; Vetere, V. Preparation and characterization of a supported system of Ni2P/Ni12P5 nanoparticles and their use as the active phase in chemoselective hydrogenation of acetophenone. *Nanotechnology* **2018**, *29*, 215702. [CrossRef]
30. Su, N.; Gao, X.Y.; Chen, X.Y.; Yue, B.; He, H.Y. The enantioselective hydrogenation of acetophenone over Pd concave tetrahedron nanocrystals affected by the residual adsorbed capping agent polyvinylpyrrolidone (PVP). *J. Catal.* **2018**, *367*, 244–251. [CrossRef]
31. Yang, X.K.; Ding, H.X.; Ren, Y.H.; Kang, Y.K.; Li, Y.F.; Li, Z.H.; Yue, B.; He, H.Y.; Chen, X.Y. Facet-dependent catalytic activity of shape-controllable palladium nanocrystals with clean surface in acetophenone selective hydrogenation. *J. Catal.* **2023**, *428*, 115159. [CrossRef]
32. Xia, X.H.; Xie, S.F.; Liu, M.C.; Peng, H.C.; Lu, N.; Wang, J.G.; Kim, M.J.; Xia, Y.N. On the role of surface diffusion in determining the shape or morphology of noble-metal nanocrystals. *Proc. Nat. Acad. Sci. USA* **2013**, *110*, 6669–6673. [CrossRef] [PubMed]
33. Dachraoui, W.; Bodnarchuk, M.I.; Vogel, A.; Kovalenko, M.V.; Erni, R. Unraveling the shell growth pathways of Pd-Pt core-shell nanocubes at atomic level by in situ liquid cell electron microscopy. *Appl. Phys. Rev.* **2021**, *8*, 041407. [CrossRef]
34. Chen, H.Y.T.; Chou, J.P.; Lin, C.Y.; Hu, C.W.; Yang, Y.T.; Chen, T.Y. Heterogeneous Cu-Pd binary interface boosts stability and mass activity of atomic Pt clusters in the oxygen reduction reaction. *Nanoscale* **2017**, *9*, 7207–7216. [CrossRef] [PubMed]
35. Roh, G.; Lee, H.; Jeong, Y.; Kim, J.H.; Kim, H. Preparation of carbon-supported Pt-Ru core-shell nanoparticles using carbonized polydopamine and ozone for a CO tolerant electrocatalyst. *Int. J. Hydrogen Energ.* **2019**, *44*, 21588–21596. [CrossRef]
36. Kibis, L.S.; Titkov, A.I.; Stadnichenko, A.I.; Koscheev, S.V.; Boronin, A.I. X-ray photoelectron spectroscopy study of Pd oxidation by RF discharge in oxygen. *Appl. Surf. Sci.* **2009**, *255*, 9248–9254. [CrossRef]
37. Crist, B.V. *Handbook of Monochromatic XPS Spectra, the Elements of Native Oxides*; John Wiley & Sons: Hoboken, NJ, USA, 2000; Volume 1, pp. 278–280.
38. Kibis, L.S.; Stadnichenko, A.I.; Koscheev, S.V.; Zaikovskii, V.I.; Boronin, A.I. Highly oxidized palladium nanoparticles comprising Pd4+ species: Spectroscopic and structural aspects, thermal stability, and reactivity. *J. Phys. Chem. C* **2012**, *116*, 19342–19348. [CrossRef]
39. Tian, X.L.; Zhao, X.; Su, Y.Q.; Wang, L.J.; Wang, H.M.; Dang, D.; Chi, B.; Liu, H.F.; Hensen, E.J.M.; Lou, X.W.; et al. Engineering bunched Pt-Ni alloy nanocages for efficient oxygen reduction in practical fuel cells. *Science* **2019**, *366*, 850–856. [CrossRef]
40. Huang, J.; Jiang, Y.J.; van Vegten, N.; Hunger, M.; Baiker, A. Tuning the support acidity of flame-made Pd/SiO2-Al2O3 catalysts for chemoselective hydrogenation. *J. Catal.* **2011**, *281*, 352–360. [CrossRef]
41. Bernardin, V.; Vanoye, L.; Rivera Cárcamo, C.; Serp, P.; Favre Réguillon, A.; Philippe, R. Acetophenone hydrogenation and consecutive hydrogenolysis with Pd/CNT catalysts: Highlighting the synergy between single atoms and nanoparticles by kinetic modeling. *Catal. Today* **2023**, *422*, 114196. [CrossRef]
42. Ghosh Chaudhuri, R.; Paria, S. Core/shell nanoparticles: Classes, properties, synthesis mechanisms, characterization, and applications. *Chem. Rev.* **2012**, *112*, 2373–2433. [CrossRef] [PubMed]
43. Lima, F.H.B.; Zhang, J.; Shao, M.H.; Sasaki, K.; Vukmirovic, M.B.; Ticianelli, E.A.; Adzic, R.R. Catalytic activity−d-band center correlation for the O_2 reduction reaction on platinum in alkaline solutions. *J. Phys. Chem. C* **2007**, *111*, 404–410. [CrossRef]

Disclaimer/Publisher's Note: The statements, opinions and data contained in all publications are solely those of the individual author(s) and contributor(s) and not of MDPI and/or the editor(s). MDPI and/or the editor(s) disclaim responsibility for any injury to people or property resulting from any ideas, methods, instructions or products referred to in the content.